2020年11月12日(木)

E会場

インターナショナル sess.

[1E01-03] インターナショナル sess. 1
司会:村山 徹(東京都立大学)
09:30 ～ 10:30 E会場 (3F・中会議室E1-2)

[1E01] ギ酸を液体キャリアとして利用した水素の貯蔵放出のための金属触媒ナノエンジニアリング
○森 浩亮[1] （1. 大阪大学大学院工学研究科）
09:30 ～ 10:00

[1E02] Cu配位構造に着目した CO_2からのメタノール合成触媒の開発
○多田 昌平[1]、大塚 文人[2]、菊地 隆司[2] （1. 茨城大学大学院、2. 東京大学大学院）
10:00 ～ 10:15

[1E03] 超臨界水中におけるリグノセルロース系バイオマスの芳香族化合物への変換反応に対する白金触媒の担体効果
○山崎 清行[1]、佐々木 隆仁[2]、渡邉 竜也[2]、桑野 聡子[2]、三村 直樹[1]、佐藤 修[1]、山口 有朋[1] （1. 国立研究開発法人　産業技術総合研究所、2. 東北学院大学）
10:15 ～ 10:30

インターナショナル sess.

[1E04-06] インターナショナル sess. 2
司会:吉川 琢也(北海道大学)
10:45 ～ 11:30 E会場 (3F・中会議室E1-2)

[1E04] 貴金属担持酸化ニオブを用いたアンモニア選択触媒酸化における担体の酸点の役割
○Lin Mingyue[1]、An Baoxiang[1]、武井 孝[1]、宍戸 哲也[1]、石田 玉青[1]、春田 正毅[1]、村山 徹[1,2] （1. 東京都立大学大学、2. Yantai University）
10:45 ～ 11:00

[1E05] **Reductive Amination of HMF over Beta Zeolite-supported Ruthenium bimetallic Catalyst**
○Xinyue Li[1], Son Dinh Le[1], Shun Nishimura[1] （1. Japan Advanced Institute of Science and Technology）
11:00 ～ 11:15

[1E06] 金属間化合物触媒上で進行する水素によるクロロフルオロアルケンの脱塩素の反応機構
○高山 大鑑[1]、有山 悟史[1]、山田 拓[2]、小松 隆之[1] （1. 東京工業大学、2. AGC株式会社）
11:15 ～ 11:30

インターナショナル sess.

[1E07-09] インターナショナル sess. 3
司会:高山 大鑑(東京工業大学)
13:00 ～ 14:00 E会場 (3F・中会議室E1-2)

[1E07] 不飽和化合物水素化用 Ni-Ir合金触媒の開発
○田村 正純[1] （1. 大阪市立大学）
13:00 ～ 13:30

[1E08] Hydroxyapatite supported polyvinylpyrrolidone-capped CuPd bimetallic catalyst for highly selective γ-butyrolactone *via* hydrogenation of succinic acid
○Son Dinh Le[1], Shun Nishimura[1] （1. Graduate School of Advanced Science and Technology, Japan Advanced Institute of Science and Technology）
13:30 ～ 13:45

[1E09] 超高耐久性を示すプロパン脱水素触媒の開発
中谷 勇希[1]、清水 研一[1]、○古川 森也[1] （1. 北海道大学触媒科学研究所）
13:45 ～ 14:00

インターナショナル sess.

[1E10-11] インターナショナル sess. 4
司会:西村 俊(北陸先端科学技術大学院大学)
14:15 ～ 15:00 E会場 (3F・中会議室E1-2)

[1E10] Synthesis of zeolitic Mo-doped vanadotungstate materials with tailorable oxidability and acidity
○Tao Meilin[1]、Ishikawa Satoshi[1]、Ueda Wataru[1] （1. Faculty of engineering, department of material and life chemistry, Kanagawa University）
14:15 ～ 14:30

[1E11] 酸化物ナノシートを用いたナノ構造触媒の開発
○伊田 進太郎[1] （1. 熊本大学産業ナノマテリアル研究所）
14:30 ～ 15:00

2020年11月13日(金)

E会場

インターナショナル sess.

[2E01-03] インターナショナル sess. 5
司会:三浦 大樹(東京都立大学)
09:00 ～ 09:45 E会場 (3F・中会議室E1-2)

[2E01] ZSM-5担持 Rh二元機能触媒を用いた*n*-ヘキサン接触分解の低温化
○藤墳 大裕[1]、山地 真愛[1]、多湖 輝興[1] （1. 東京工業大学物質理工学院）
09:00 ～ 09:15

[2E02] 高次な構造を有する Moおよび W酸化物触媒の合成と酸化触媒能
○下田 光祐[1]、宮沢 真維[1]、石川 理史[1]、上田 渉[1] （1. 神奈

川大学工学部物質生命化学科）

09:15 ～ 09:30

[2E03] フェノキシ配位ハーフチタノセン触媒によるエチレン共重合：活性への配位子効果

○Kitphaitun Suphitchaya[1]、野村 琴広[1]（1. 東京都立大学理学研究科 化学専攻）

09:30 ～ 09:45

インターナショナル sess.

[1E01-03] インターナショナル sess. 1

司会:村山 徹(東京都立大学)

2020年11月12日(木) 09:30 ～ 10:30 E会場 (3F・中会議室E1-2)

[1E01] ギ酸を液体キャリアとして利用した水素の貯蔵放出のための金属触媒ナノエンジニアリング

○森 浩亮[1] （1. 大阪大学大学院工学研究科）

09:30 ～ 10:00

[1E02] Cu配位構造に着目した CO_2からのメタノール合成触媒の開発

○多田 昌平[1]、大塚 文人[2]、菊地 隆司[2] （1. 茨城大学大学院、2. 東京大学大学院）

10:00 ～ 10:15

[1E03] 超臨界水中におけるリグノセルロース系バイオマスの芳香族化合物への変換反応に対する白金触媒の担体効果

○山崎 清行[1]、佐々木 隆仁[2]、渡邉 竜也[2]、桑野 聡子[2]、三村 直樹[1]、佐藤 修[1]、山口 有朋[1] （1. 国立研究開発法人　産業技術総合研究所、2. 東北学院大学）

10:15 ～ 10:30

Nano-catalyst Engineering for Storage and Release of Hydrogen Energy Using Formic Acid as a Promising Liquid Carrier

(Osaka Univ.* ・ESICB Kyoto University**) ○Kohsuke Mori*,**

1. Introduction

Formic acid (FA, HCOOH) has emerged as one of the most promising hydrogen storage compounds because it has a high gravimetric capacity for hydrogen (4.4 wt%), is relatively nontoxic and is a nonflammable liquid under ambient conditions. Additionally, the use of FA could allow economical CO_2-mediated hydrogen storage energy cycling via the regeneration of FA through the hydrogenation of CO_2. Thus the development of reliable heterogeneous catalysts targeted to both FA dehydrogenation and FA synthesis is an urgent yet challenging task. Herein the state of the art in the exploitation of promising nano-catalysts designed by surface and interface engineering with atomic precision for this targeted reaction are presented, which further provides the precise catalytic site design protocols.

2. Hydrogen production from FA

The decomposition of FA by selective dehydrogenation ($HCOOH \rightarrow H_2 + CO_2$) is thermodynamically favored (ΔG = -48.4 kJ mol^{-1}). It is desirable to completely suppress the side reaction $HCOOH \rightarrow CO + H_2O$ (ΔG = -28.5 kJ mol^{-1}), because the generated CO is both highly toxic and capable of poisoning Pt fuel cell catalysts. For the practical reason of on-board application, current research has been focused on the exploitation of efficient heterogeneous catalysts. Bering this in mind, we have developed the heterogeneous nano-catalysts, such as PdAg, PdAu, PdCu, PdCuCr, for the efficient production of high-purity H_2 from FA dehydrogenation [1-5].

PdAg nanoparticles supported on phenylamine-functionalized mesoporous carbon (MSC) were synthesized as a heterogeneous catalyst (**Fig. 1A**) [6]. The PdAg NPs were evidently well dispersed and had a narrow size distribution, with an average diameter of 1.2 nm (**Fig. 1B**). The Pd 3d peaks in XPS analysis generated by the PdAg/amine-MSC was shifted to lower binding energies than that of the corresponding monometallic Pd catalysts. This outcome is attributed to the ability of Ag atoms to donate electrons to Pd atoms after alloying, based on their electronegativity values of 1.93 and 2.20.

A remarkably high turnover frequency (TOF) of 5638 h^{-1} was obtained during the dehydrogenation of FA, corresponding to an outstanding reaction rate of 1,070,000 $mL \cdot h^{-1} \cdot g_{Pd}^{-1}$. It should be noted that the present catalytic system can suppress unfavorable CO contamination from the dehydration pathway ($HCOOH \rightarrow H_2O + CO$) less than detection limit by GC (1 ppm). The Ag catalyst did not show any activity (data not shown), while the catalytic performance of the PdAg was higher than that of the monometallic Pd analogue (**Fig. 1C**).

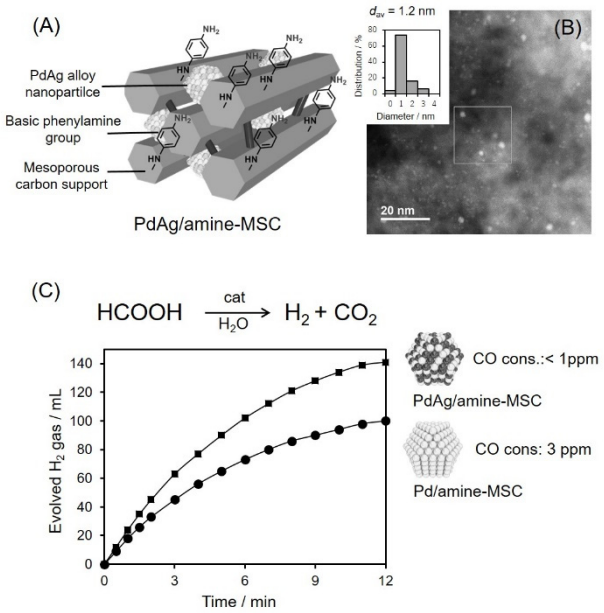

Fig. 1 (A) Illustartion of PdAg/amine-MSC, (B) HAADF-STEM image and size distribution plot, and (C) time profile in the FA dehydrogenation.

In the dehydrogenation of FA, the reaction is initiated by the O-H bond cleavage to form metal-formate species (Step 1) (**Fig. 2**). Such metal-formate species undergo the isomerization (Step 2), and evolve metal hydride and CO_2 via β-hydride elimination (Step 3). The catalytic cycle concludes with the regeneration of the catalysts accompanied with the formation of H_2 (Step 4). To better understand the role of the amine functional groups and the alloying, potential energy profiles were generated using DFT calculations, employing a $Pd_{11}Ag_{11}$ cluster as a model for alloy NPs.

In the presence of phenylamine, the formation of $HCOOH–PhNH_2$ appears reasonable as a result of the acid-base interaction, and $HCOO^-$ is spontaneously generated without any transition state. On the other hand,

the activation energy was deteremiend to 11.9 kcal/mol to produce the formate ($HCOO^-$) intermediate in the absence of amine group. Moreover, H_2 production occurs with a barrier of 7.8 kcal/mol in the presence of phenylamine, which is substantially lower than the value of 23.0 kcal/mol calculated in the absence of the amine. It can be concluded that both the O–H bond dissociation and the H_2 desorption steps are enhanced by the presence of neighboring amine functional groups.

The activation energies for each elementary steps over the Pd22 cluster model were determined to be 20.0, 15.2, 16.6 and 24.6 kcal/mol for steps 1 - 4, respectively. Alloying Pd with Ag changes the electron density at the active Pd sites due to charge transfer from Ag to Pd resulting from the different work functions of the two elements, which facilitate the O–H and C–H bond dissociation steps. Kinetic Isotope Effect (KIE) using HCOOH, HCOOD and DCOOH also support such results.

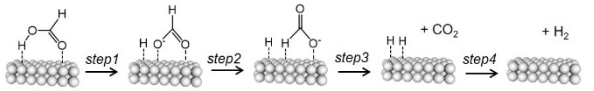

	Step 1 O-H dissociation	Step 2 Isomerization	Step 3 C-H dissociation	Step 4 H_2 production
Pd	20.0	15.2	16.6	24.6
PdAg	11.9	13.5	11.0	23.0
PdAg + amine	0.1	14.2	9.3	7.8

/kcal·mol-1

Fig. 2 A possible reaction pathway and activation enetgies for dehydrogenation to FA over Pd22 and Pd11Ag11 cluster models determined by DFT calculations.

More recently, we demonstrate the selective production of hydrogen isotope compounds from a combination of formic acid and D_2O, through cooperative action by a PdAg nanocatalyst on a silica substrate whose surface is modified with amine groups (**Fig. 3**) [7]. In this process, D_2 is predominantly evolved by the assist of weakly basic amine moieties, while nanocatalyst particles in the vicinity of strongly basic amine groups promote the preferential formation of HD. Kinetic data and calculations based on semi-classically corrected transition state theory coupled with density functional theory suggest that quantum tunneling dominates the hydrogen/deuterium exchange reaction over the metallic PdAg surfaces.

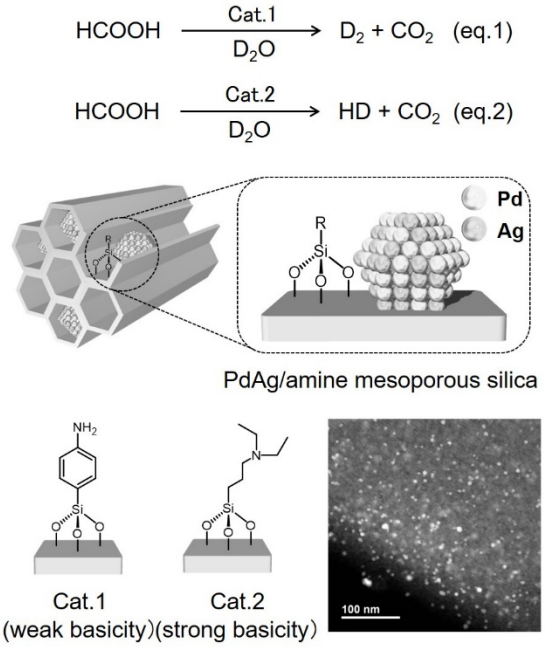

Fig. 3 Controlled release of hydrogen isotope compounds from the dehydrogenation of FA in D_2O using amine functionalized PdAf catalyst.

3. FA synthesis from CO_2 Hydrogenation

The gas phase hydrogenation of CO_2 to produce formic has a positive free energy change (CO_2 (g) + H_2 (g) → HCOOH (l), ΔG = +33 kJ mol^{-1}). Conventionally, the reaction is performed in an aqueous condition by the addition of a weak base, such as a tertiary amine or alkali/alkaline earth bicarbonate, which enable the shift of thermodynamic equilibrium to the product side (CO_2 (aq) + H_2 (aq) + B → HCO_2^- (aq) + BH^+ (B: base), ΔG = −35.4 kJ mol^{-1}) [8]. Unfortunately, the advance of heterogeneous catalysts lags considerably in spite of the noticeable practical benefits even in the industrial application.

The precise tuning of the surface composition of PdAg nanoparticles was performed to investigate the effect of surface-exposed active Pd atoms in alloy NPs [9]. The co-reduction of Pd and Ag precursors conventionally afford random PdAg alloy nanoparticles ($PdAg/TiO_2$) By applying a surface engineering approach via the successive reduction of metal precursors, $Pd@Ag/TiO_2$ with a $Pd_{core}Ag_{shell}$ structure and $Ag@Pd/TiO_2$ with an $Ag_{core}Pd_{shell}$ structure were synthesized.

PdAg alloy nanoparticles supported on TiO_2 was proven to be an efficient selective hydrogenation catalyst of CO_2 100 °C under relatively low pressure condition (2.0 MPa, CO_2/H_2 =1). The $Pd@Ag/TiO_2$ exhibited an

elevated TON (2,496) based on the total quantities of Pd employed despite the low density of surface exposed Pd atoms. As expected, a maximum TON value of 14839 was obtained from the Pd@Ag/TiO_2 based on the quantity of surface Pd atoms, which was determined by pulsed CO adsorption measurements, This TON value is a more than ten times higher than that of the monometallic Pd/TiO_2. Moreover, a well correlation between the TON based on surface Pd atoms and the Pd $3d_{5/2}$ binding energy determined by XPS analysis evidently observed.

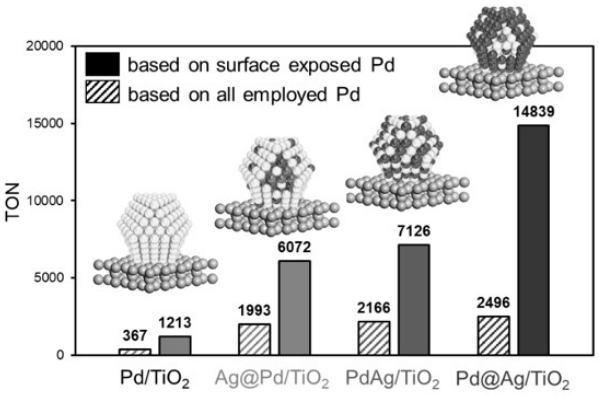

Fig. 4 Comparison of the catalytic activities of a series of supported PdAg catalysts with different surface compositions and Pd/TiO_2 during CO_2 hydrogenation.

The CO_2 hydrogenation over Pd_{22} is initiated by the dissociation of H_2 to form a metal-hydride species via $TS_{I/II}$ with a barrier of 13.9 kcal/mol (*step 1*). Next, the adsorption of HCO_3^- to produce intermediate III (*step 2*), followed by the attack of H atom to the C atom of HCO_3^- via $TS_{III/IV}$, with a barrier of 77.4 kcal/mol (*step 3*). Finally, the formate is produced accompanied by H_2O regenerates the initial active species (*step 4*). The activation energies for *step 1* using $Pd_{11}Ag_{11}$ and Pd_6Ag_{16} clusters, were 11.9 and 11.0 kcal/mol, respectively, which were similar to that obtained with the Pd_{22}. On the other hand, the reduction of HCO_3^- via $TS_{III/IV}$ occurs with a barrier of 58.7 and 46.2 kcal/mol for $Pd_{11}Ag_{11}$ and Pd_6Ag_{16}, respectively. These results show that the rate-determining step is *step 3*, and further demonstrate that the importance of low Pd/Ag ratio of the PdAg alloy nanoparticles in boosting the rate-determining step.

We have recently elucidated the positive effects imparted by the interfacial modification of PdAg/TiO_2 with ZIF-8 during CO_2 hydrogenation to FA [10, 11]. Moreover, a PdAg catalyst on a hydrophilic N-doped polymer-silica composite support was proven to be active for the CO_2 hydrogenation reaction under additive-free aqueous conditions to produce pure formic acid (CO_2 (aq) + H_2 (aq) → HCOOH (aq), $\Delta G = -4$ kJ mol^{-1}) [12]. High hydrophilic nature and the higher CO_2 adsorption capacity at low temperatures compared to metal oxide supports may have contributed to the increased activity.

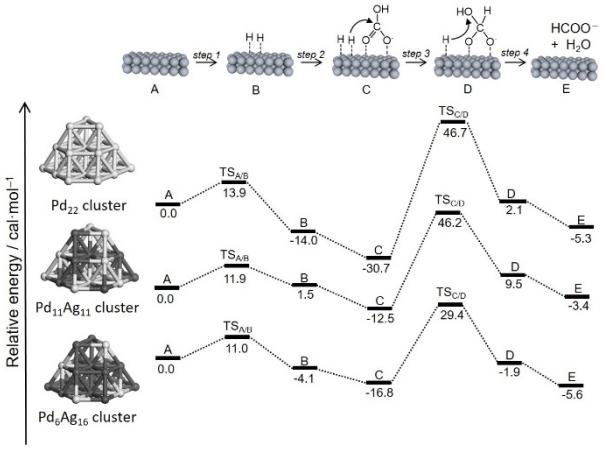

Fig. 5 Possible reaction mechanism for CO_2 hydrogenation to formic acid and potential energy profiles as determined by DFT calculations.

1) K. Mori, M. Dojo, H. Yamashita, *ACS Catal.*, **3**, 1114 (2013).
2) K. Mori, H. Tanaka, M. Dojo, K. Yoshizawa, H. Yamashita, *Chem. Eur. J.*, **21**, 12085 (2015).
3) K. Mori, K. Naka, S. Masuda, K. Miyawaki, H. Yamashita, *ChemCatChem*, **9**, 3456 (2017).
4) K. Mori, S. Masuda, H. Tanaka, K. Yoshizawa, M. Che, H. Yamashita, *Chem. Commun.*, **53**, 4677 (2017).
5) M. Wen, K. Mori, Y. Kuwahara, H. Yamashita, *ACS Energy Lett.*, 2, 1 (2017).
6) S. Masuda, K. Mori, Y. Futamura, H. Yamashita, *ACS Catal.*, **8**, 2277 (2018).
7) K. Mori, Y. Futamura, S. Masuda, H. Kobayashi, H. Yamashita, *Nat. Commun.*, **10**, 4094 (2019).
8) K. Mori, T. Taga, H. Yamashita, *ACS Catal.*, **7**, 3147 (2017).
9) K. Mori, T. Sano, H. Kobayashi, H. Yamashita, *J. Am. Chem. Soc.*, **140**, 8902 (2018).
10) M. Wen, K. Mori, Y. Futamura, Y. Kuwahara, M. Navlani-García, T. An, and H. Yamashita, *Sci. Rep.*, **9**, 15675 (2019).
11) K. Mori, A. Konishi, H. Yamashita, *J. Phys. Chem. C*, **124**, 11499 (2020).
12) S. Masuda, K. Mori, Y. Kuwahara, C. Louis, H. Yamashita, *ACS Appl. Energy Mater.*, **3**, 5847 (2020).

CO_2-to-methanol hydrogenation catalyst by focusing on coordination structure of Cu species

(Ibaraki Univ. *, Univ. Tokyo**) ○Shohei Tada*, Fumito Otsuka**, Ryuji Kikuchi**

1. Introduction

Recently, the catalyst development for CO_2 hydrogenation to methanol has attracted attention. Many researchers have been investigating Cu-based catalysts to improve catalytic activity. We focused on the metal nanoparticle formation by the deposition-reduction method. After H_2 reduces the metal-containing mixed oxides, the metal nanoparticles will be selectively formed. We considered that a spinel-type oxide $Mg_{1-x}Cu_xAl_2O_4$ is a promising catalyst specific to the CO_2 hydrogenation. It is a basic metal oxide, which can activate CO_2 adsorbed on its surface. Furthermore, it has a high specific surface area, which will increase the number of active sites.

In this study, we investigated the mechanism of Cu nanoparticle formation *via* the deposition-reduction method over $Mg_{1-x}Cu_xAl_2O_4$.

2. Experimental

$Mg_{1-x}Cu_xAl_2O_4$ was prepared by the Pechini method. Ethylene glycol (Wako) and citric acid (Sigma-Aldrich) were stirred at 200 °C and homogenized. The molar ratio of ethylene glycol to citric acid was 4. Stoichiometric amounts of $Mg(NO_3)_2{\cdot}6H_2O$ (Wako), $Al(NO_3)_3{\cdot}9H_2O$ (Wako), $Cu(NO_3)_2{\cdot}3H_2O$ (Wako) were added to the obtained solution at 80 °C. The solution was heated at 200 °C, resulting in the powder formation. The crude powder was calcined at 800 °C for 4 h. The obtained catalysts were characterized by temperature-programmed reduction of H_2 (H_2-TPR), ^{27}Al MAS-NMR, XAS, and EPR.

3. Results and Discussion

H_2-TPR was conducted using $Mg_{1-x}Cu_xAl_2O_4$ to evaluate their reducibility (Figure 1). First, we estimated their Cu loading assuming that the peak corresponds to Cu^{2+} reduction to Cu^0. The Cu loading is almost the same as that calculated from the stoichiometric ratio of Cu to Mg and Al, namely x, as summarized in Table 1. Therefore, we can conclude that the peak corresponds to the reduction of Cu^{2+}. Second, we focused on the low-temperature peaks. When x increases from 0.2 to 0.8, the following three features are observed. (1) the α peak does not change. (2) a shoulder peak (denoted as the β peak) appears and grows next to the α peak. (3) with increasing x, the high-temperature peak (denoted as the γ peak) becomes strong. Thus, we can conclude that $Mg_{1-x}Cu_xAl_2O_4$ contains three types of Cu^{2+} species. Besides, their proportions are related to the value of x (Table 1). Based on the difference in reducibility, we can classify the following three types of Cu^{2+} species: short O-Cu octahedral coordination, elongated O-Cu octahedral coordination, and tetrahedral coordination. The reason for this classification will be discussed.

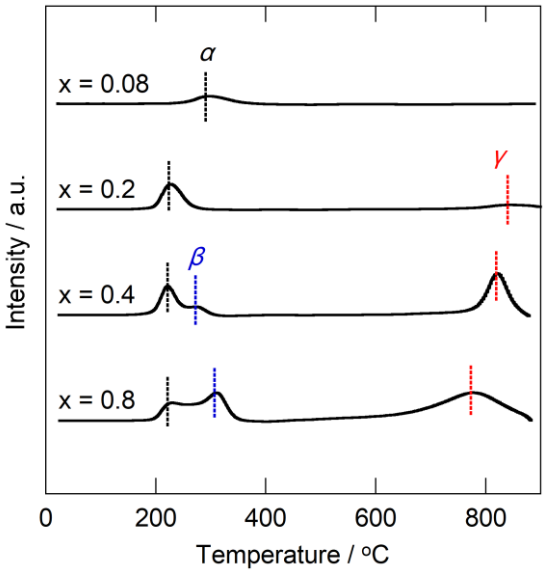

Figure 1 H_2-TPR profiles of $Mg_{1-x}Cu_xAl_2O_4$.

Table 1 Peak area in H_2-TPR profiles and estimated Cu loading.

x	Peak area in H_2-TPR profile [a.u.]				Cu loading [wt%]	
	α	β	γ	Sum	x [a]	H_2-TPR [a]
0.08	134	0	0	134	3.5	2.4
0.2	280	0	137	417	8.5	7.3
0.4	265	73	565	903	16	16
0.8	228	389	1110	1727	29	30

[a] The value was used to calculate the Cu loading.

Acknowledgements This work was supported by the Japan Petroleum Institute, Japan, and the Japan Society for the Promotion of Science (JSPS) KAKENHI, Japan (No. 18K04838).

Effects of supports for Pt-based catalysts on conversion of lignocellulosic biomass into aromatic monomers in supercritical water

（AIST*・Tohoku Gakuin University**）○Kiyoyuki Yamazaki*・Ryuto Sasaki**・Tatsuya Watanabe**・Satoko Kuwano**・Naoki Mimura*・Osamu Sato*・Aritomo Yamaguchi*

1. Introduction

Utilization of biomass is effective to realize carbon neutral and sustainable society. Lignin is one of the three components of lignocellulosic biomass as well as cellulose and hemicellulose. Lignin consists of cross-linked aromatic compounds and aromatics can be obtained by depolymerization of lignin.[1]

Lignin conversion to simple aromatic monomers is attractive as an alternative process of conventional reforming from oil resources. In previous works, charcoal supported Pt catalyst was found to be more active than any other charcoal supported metal catalysts for the conversion of biomass to aromatic monomers (Yield=17.4 %).[2] In this study, we considered effects of supports and improved the yield using Pt-based catalysts in supercritical water (Fig.1).

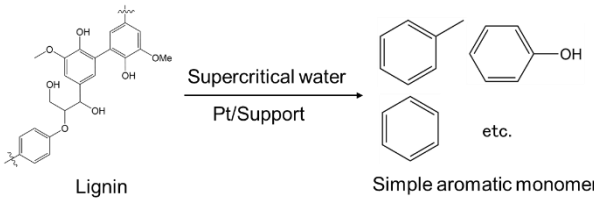

Fig.1 Lignin conversion over supported Pt catalysts

2. Experimental

Supported Pt-based catalysts were prepared as follows. HNO_3 solution of $[Pt(NO_2)_2(NH_3)_2]$, support, and water were put into a flask and stirred overnight. After evaporation of the solvent, obtained powder was reduced with hydrogen in a furnace at 473 K. Then, supported Pt-based catalyst was obtained. The ratio of Pt in Pt-based catalysts was 5wt%.

Lignin conversion was carried out in a batch reactor. Catalyst 0.15 g, Japanese cedar 0.20 g, and water 3.0 g were put into the reactor. Then, the reactor was purged with argon gas and heated at 673 K for 1 h. Gaseous and liquid products were collected and analyzed by gas chromatograph. Solid products were recovered and weighed. Yields of products from lignin conversion were calculated by dividing moles of aromatic compounds in products by moles of aromatic rings in initial biomass.

3. Results and Discussions

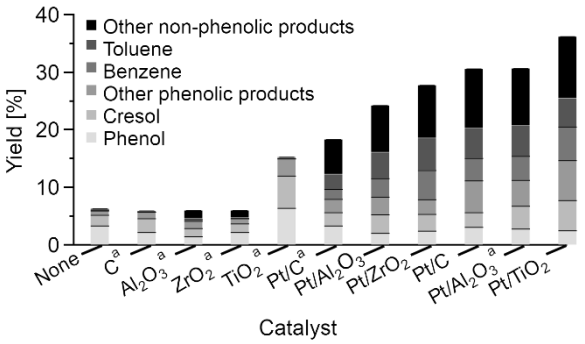

Fig.2 Yields of aromatic products from Japanese cedar (a: commercially available)

Fig.2 shows yields of aromatic products in the presence or absence of synthesized or commercial supported Pt catalysts. Various aromatic monomers could be produced by this reaction. Among the catalyst supports (C, Al_2O_3, ZrO_2, and TiO_2), TiO_2 showed catalytic performance even without Pt. Considering the support of the catalyst, TiO_2 was found to be the most effective support in this reaction and the yield was improved up to 36.2 %.

1. J. Zakzeski, et.al., *Chem. Rev.* **2010,** *110*, 3552.
2. A. Yamaguchi, et.al., *Mol. Catal.* **2019,** *477*, 6.

インターナショナル sess.

[1E04-06] インターナショナル sess. 2

司会:吉川 琢也(北海道大学)

2020年11月12日(木) 10:45 〜 11:30 E会場 (3F・中会議室E1-2)

[1E04] 貴金属担持酸化ニオブを用いたアンモニア選択触媒酸化における担体の酸点の役割

○Lin Mingyue[1]、An Baoxiang[1]、武井 孝[1]、宍戸 哲也[1]、石田 玉青[1]、春田 正毅[1]、村山 徹[1,2]（1. 東京都立大学大学、2. Yantai University）

10:45 〜 11:00

[1E05] Reductive Amination of HMF over Beta Zeolite-supported Ruthenium bimetallic Catalyst

○Xinyue Li[1], Son Dinh Le[1], Shun Nishimura[1]（1. Japan Advanced Institute of Science and Technology）

11:00 〜 11:15

[1E06] 金属間化合物触媒上で進行する水素によるクロロフルオロアルケンの脱塩素の反応機構

○高山 大鑑[1]、有山 悟史[1]、山田 拓[2]、小松 隆之[1]（1. 東京工業大学、2. AGC株式会社）

11:15 〜 11:30

Role of acid sites for selective catalytic oxidation of NH_3: the case of niobium oxide supported precious metals catalysts

(Tokyo Metropolitan University[*1], Yantai University[*2])
○Mingyue Lin[*1], Baoxiang An[*1], Takashi Takei[*1], Tetsuya Shishido[*1], Tamao Ishida[*1], Masatake Haruta[*1], Toru Murayama[*1,2]

1. Introduction

Ammonia is a strong N-containing odor that has negative impacts on human health and the environment. Selective catalytic oxidation (SCO) of NH_3 to N_2 and H_2O is an ideal method for its removal.

NH_3, as an odor gas which has negative impacts on human health and the environment, it is essential and important to develop efficient method to remove it.

Selective catalytic oxidation (SCO) of NH_3 to N_2 and H_2O is an ideal method. However, the developed catalysts either need high reaction temperatures or produce non-environmental-friendly byproduct of N_2O. In this study, we reported the role of acid sites for highly selective catalytic oxidation of NH_3 to N_2 over niobium oxide supported precious metals (Pt, Pd, and Au) catalysts (>95% at the full conversion), which will provide a new concept for the design of catalysts for NH_3-SCO with high N_2 selectivity.

2. Experimental

Nb_2O_5 was synthesized by a hydrothermal synthesis and calcined at 400°C. [1] Au/Nb_2O_5 was prepared by a sol immobilization method. [1] Pt/Nb_2O_5 and Pd/Nb_2O_5 were prepared by impregnation method. [2] The loading amount of precious metals was prepared as 1wt%. NaOH treatment was carried out by adding 1 mol L^{-1} NaOH (10 mL) to the catalyst and the mixture was stirred for 1 h. After thoroughly washed by deionized water, the resulting solid was dried at 120°C overnight.

The catalytic activity test was carried out on a fixed-bed reactor system connected with an FI-IR. The inlet gas contained 50 ppm NH_3, 20% O_2, and Ar balance. The total flow rate is 100 mL min^{-1} and the catalyst amount was 0.15 g.

3. Results and Discussion

Niobium oxide obtained from the hydrothermal synthesis shows a deformed orthorhombic structure and its BET surface area was 208 m^2/g. The total acid amount calculated from NH_3-TPD measurements was 0.37 mmol/g and it possessed both Brønsted and Lewis acid sites according to the pyridine adsorption.

The effects of solid acidity of the Nb_2O_5 support on NH_3-SCO were investigated by using NaOH to neutralize the Brønsted acid sites of Nb_2O_5. As shown in Figure 1, Au/Nb_2O_5, Pt/Nb_2O_5, and Pd/Nb_2O_5 showed very high N_2 selectivities along with the increasing NH_3 conversions and they showed 95%, 98%, and 100% N_2 selectivity at the full NH_3 conversion, respectively. After NaOH treatment the N_2 selectivities of Au/Nb_2O_5, Pt/Nb_2O_5, and Pd/Nb_2O_5 decreased significantly which decreased to 32%, 74%, and 74% at the full conversion of NH_3, respectively. These results strongly indicated that the Brønsted acid sites are important for improving the N_2 selectivity of NH_3-SCO.

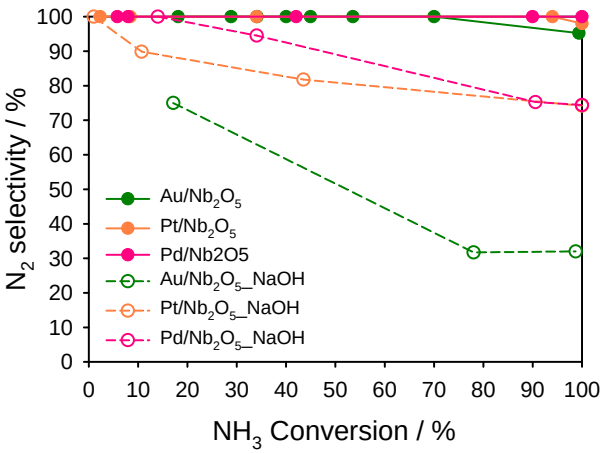

Figure 1. Effect of NaOH treatment on NH_3 conversion and N_2 selectivity over Au/Nb_2O_5, Pt/Nb_2O_5, and Pd/Nb_2O_5.

1) M. Lin, B. An, N. Niimi, Y. Jikihara, T. Nakayama, T. Honma, T. Takei, T. Shishido, T. Ishida, M. Haruta, T. Murayama, *ACS Catal.*, 9(3), 1753 (2019)
2) M. Lin, B. An, T. Takei, T. Shishido, T. Ishida, M. Haruta, T. Murayama, *J. Catal.*, 389, 366-374 (2020).

Reductive amination of HMF over beta zeolite-supported ruthenium bimetallic catalyst

(JAIST) ○LI, Xinyue・LE, Dinh Son・NISHIMURA, Shun

1. Introduction

The ever-increasing industrial production of commodity and specialty chemicals inexorably depletes the finite primary fossil resources available on Earth. Consequently, for the sustainable development, effective transformations of renewable biomass, which is a virtually inexhaustible reservoir, to fuels and chemical building blocks are envisaged.[1] The 5-hydroxymethyl-2-furaldehyde (HMF) is a great platform chemical produced from lignocellulosic biomass, and enables various successive transformations to value-added compounds. Herein, the reductive amination of HMF over various beta zeolite supported monometallic and bimetallic Ru catalysts, denoted as Ru/BEA and RuM/BEA, to 5-aminomethyl-2-furylmethanol (FAA) is investigated. Primary amines are important and versatile building blocks in organic synthesis because they are widely utilized as intermediates for the production of polymers, drugs, dyes, and detergents.[2-4]

2. Experimental

The catalysts were prepared by an impregnation method with various BEA composed with different Si/2Al ratios (42.4, 104, 150, 440, and 1700). To evaluate the catalytic performance, HMF (1 mmol), 25% NH_3 aq. (3 mL), and ethanol (3 mL) were mixed in a stainless-steel autoclave with a Teflon inter tube (50 mL vol.). After addition of as-prepared catalyst (10 mg) and filling with H_2 gas (0.6 MPa), the reaction was performed at 100 °C under vigorous stirring. The reaction media is analyzed by a GC-FID equipped with a nonpolar DB-1 column by using 1-butanol (1 mmol) as an internal standard.

3. Results and Discussions

At first, various Ru metal loadings on BEA zeolite are surveyed at Si/2Al = 150. It is observed that increase of Ru loading leads an increase of FAA yield gradually, and then both 3wt% and 5wt% of Ru loaded BEA catalysts gave the high FAA yields of 70%.

Figure 1 (a) shows the time-based reaction progress over 3wt% monometallic Ru/BEA composed with different Si/2Al ratios. Interestingly, the Si/2Al ratio of BEA support significantly impacted the reactivity for the reductive amination of HMF. Increase of Si/2Al from 42.2 to 150 has enhanced the reactivity for FAA production, and the highest yield for FAA was obtained as 70% for 6 h reaction. While, further increase of Si/2Al lead a drastic decrease of FAA yield. Analyses of Ru-K edge XAFS (SPring-8, BL01B1 and BL14B2) indicated that smaller Ru-Ru CNs served higher yield of FAA. It is also observed that highly active Ru/BEA (Si/Al2 = 150) possesses more fraction of Ru-O than that of low active Ru/BEA (Si/2Al = 1700). According to these results, it is expected that the Si/2Al ratio of BEA support contributed to the metal-support interaction, and which played a key factor to control Ru size leading to difference in reactivity for the reductive amination of HMF to FAA.

To further enhance the reactivity of monometallic Ru/BEA catalyst and decrease the quantity of precious Ru element usage, addition of common elements such as Fe, Cu, Co and Ni constructing bimetallic RuM/BEA (Si/2Al = 150) was investigated. Remarkably, the bimetallic RuNi was found to be the superior catalyst among those combinations; which served 70% yield of FAA whereas RuFe, RuCo and RuCu presented only 17-47% yield of FAA at 12 h reaction (**Figure 1(b)**).

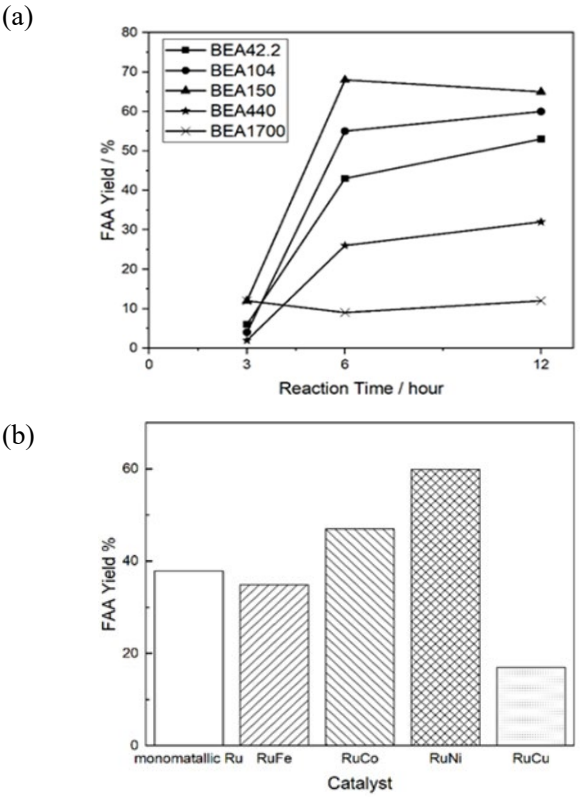

Fig. 1 Yield of FAA on the reductive amination of HMF for (a) Time-based reaction progression over the 3wt% Ru/BEA composed of different Si/2Al ratio, and (b) 12 h reaction over various RuM/BEA catalysts.

1) Gérardy *et al., Chem. Rev.* 120 (2020) 7219.
2) Nisimura *et al., Res. Chem. Intermed.* 42 (2016) 19.
3) Komanoya *et al., J. Am. Chem. Soc.* 139 (2017) 11493.
4) Dong *et al.*, *Mol Catal.* 482 (2020) 110755.

Reaction mechanism of dechlorination of chlorofluoroalkene by hydrogen gas over intermetallic compound catalysts

(Tokyo Institute of Technology 1*, AGC Inc. 2**) ○Tomoaki TAKAYAMA 1*, Satoshi ARIYAMA 1*, Taku YAMADA 2**, Takayuki KOMATSU 1*

1. Introduction

2,3,3,3-tetrafluoropropene (***H(2)***, scheme 1) has gathered much attention as an alternative automobile refrigerant to the current ones because of its lower global warming potential.[1] Dechlorination of chlorofluoroalkene, ***H(0)***, by hydrogen gas over heterogeneous Pd catalyst has been known as a protocol to provide ***H(2)***. However, by-products, ***H(3)~H(5)***, have been formed *via* the successive hydrogenation and defluorination of ***H(2)***. In contrast, we have recently discovered that Pd-based intermetallic compounds (Pd_3M; M = Bi, Pb, or In) inhibit the by-products from producing.[2] Herein, we discuss the factor affecting the selectivities to the products in the dechlorination of ***H(0)*** based on control and spectroscopic experiments.

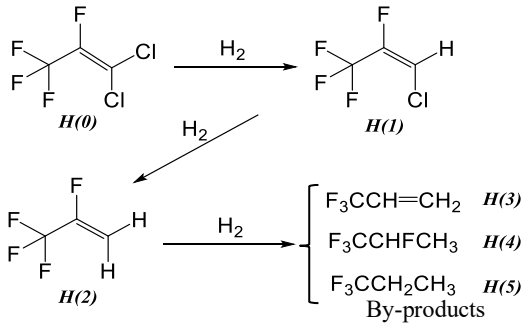

Scheme 1. Dechlorination of ***H(0)*** by hydrogen gas.

2. Experimental

The nanoparticulate monometallic Pd and intermetallic compounds Pd_3M (M = Bi, Pb, or In) were formed on SiO_2 support by co-impregnation with the conventional pore-filling protocol, followed by H_2 reduction at 400 and 800ºC. Dechlorination of ***H(0)*** was carried out by a fixed-bed flow-type stainless steel reactor (atmospheric pressure). Prior to the dechlorination reaction, the catalysts fixed on the bed were reduced by H_2 gas at 400ºC, followed by cooling to room temperature. The reaction was initiated by supplying mixed gas (***H(0)***/H_2/Ar=1/1/3.4; mole ratio) at 90 or 150ºC. The products were determined by injecting the gaseous sample extracted using a glass syringe into GC-FID.

3. Results and Discussion

Fig 1. shows influence of the conversion of ***H(0)*** on the selectivities to ***H(1)*** and ***H(2)*** formations. The selectivities over all the Pd-based intermetallic compound catalysts were greater than that over monometallic Pd catalyst. Among them, Pd_3Bi showed the highest selectivity. In other words, the formations of the by-products, ***H(3)~H(5)***, were inhibited over Pd_3Bi as compared to those on the other intermetallic compound catalysts.

We investigated the relationship between electron density of the Pd sites of the Pd-based catalyst surfaces and the by-product selectivities based on Fourier transform infrared spectroscopy using CO as the probe molecule. The sum of the selectivities to ***H(4)*** and ***H(5)*** formations were certainly decreased with red-shift of the wavenumber of the stretching vibration of CO, which could be assigned to linear adsorption of the CO molecules on the Pd sites (Fig. 2), while no relationship was observed against the sum of the ***H(3)*** and ***H(5)*** selectivities (data not shown). This suggests that the electron density of the Pd sites makes a difference in inhibition of the successive hydrogenation of the alkenyl group.

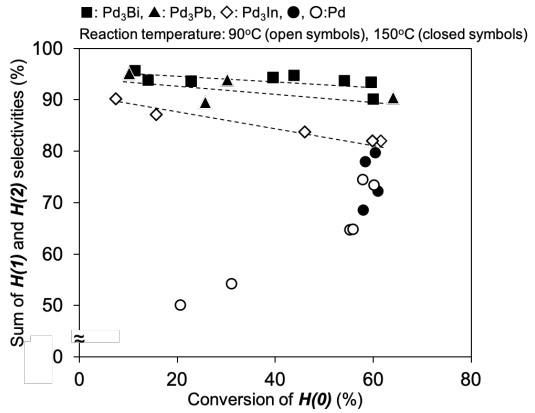

Fig. 1 Influence of the conversion of ***H(0)*** on the sum of ***H(1)*** and ***H(2)*** selectivities.

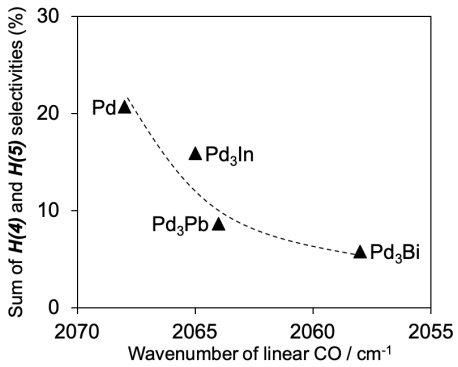

Fig. 2 Relationship between wavenumber of CO adsorbed on the Pd sites and the sum of ***H(4)*** and ***H(5)*** selectivities.

1) Calm, J. M., *Int. J. Refrig.* **31**, 1123 (2008).
2) Ariyama, S., Takayama, T., Yamada, T., Komatsu, T., 124th CATSJ Meetings Abstract, 2E11 (2019).

インターナショナル sess.

[1E07-09] インターナショナル sess. 3

司会:高山 大鑑(東京工業大学)

2020年11月12日(木) 13:00 〜 14:00 E会場 (3F・中会議室E1-2)

[1E07] 不飽和化合物水素化用 Ni-Ir合金触媒の開発

○田村 正純[1] （1. 大阪市立大学）

13:00 〜 13:30

[1E08] Hydroxyapatite supported polyvinylpyrrolidone-capped CuPd bimetallic catalyst for highly selective γ-butyrolactone *via* hydrogenation of succinic acid

○Son Dinh Le[1], Shun Nishimura[1] （1. Graduate School of Advanced Science and Technology, Japan Advanced Institute of Science and Technology）

13:30 〜 13:45

[1E09] 超高耐久性を示すプロパン脱水素触媒の開発

中谷 勇希[1]、清水 研一[1]、○古川 森也[1] （1. 北海道大学触媒科学研究所）

13:45 〜 14:00

Development of Ni-Ir alloy catalyst for hydrogenation of unsaturated compounds

（Osaka City University）○Masazumi Tamura

1. Introduction

Catalytic hydrogenation of unsaturated compounds with gaseous H_2 is widely used in petrochemical, coal chemical and fine chemical industries, and development of effective heterogeneous catalysts is highly required because of the durability, recyclability, easy separation of catalysts from the products. To achieve economic and low-energy processes, rational design and preparation of heterogeneous catalysts with high atomic efficiency are essential, and various approaches such as control of geometric and electronic structure, formation of alloys, intermetallic compounds or core-shell structures, modification of main metals with metal oxides, metal ions or organic compounds, and so on. Among these approaches, the formation of bimetallic alloys is a powerful tool for fine tuning of the activity and selectivity, and particularly, single-atom alloys (SAAs) are promising owing to the high atomic efficiency[1]. SAAs often show unique and/or superior catalytic performance in comparison with the monometallic counterparts due to the comparatively well-defined active sites as well as assisting effect of the mother metals. SAAs with noble metals such as Pd, Pt, Au single-atom alloys have been intensively developed, however, SAAs with base metals such as Ni, Cu, Co and Fe single-atom alloys are hardly reported. However, the base metals often show unique catalytic performance in organic reactions, and particularly it is well-known that Ni metal works as a good catalyst for hydrogenation reactions. In this study, we aimed at the development of effective Ni-based catalysts for hydrogenation reactions. We found that Ni single-atom in Ni-Ir alloy showed high catalytic activity and high selectivity to hydrogenation reactions of unsaturated compounds compared with the monometallic counterpart catalysts[2].

2. Experimental

Ir-Ni/SiO_2 (Ir: 4 wt%) was prepared as follows: Ir/SiO_2 was prepared by impregnating SiO_2 with H_2IrCl_6 aqueous solution, followed by drying in oven at 373 K overnight. Ni was loaded on the dried Ir/SiO_2 with aqueous $Ni(NO_3)_2$ solution in the same method as the case of Ir/SiO_2, and the obtained dried catalyst was calcined at 773 K for 3 h. The catalyst was reduced under H_2 flow (30 ml/min) at 773 K for 1 h before activity test. Appropriate amount of the reduced catalyst, styrene and methanol solvent were added into a 190 ml autoclave with an inner glass cylinder. The air was purged by flushing three times with H_2, and then the reaction was performed at 303 K and 8 MPa H_2. The products were analyzed by FID-GC and GC-MS.

3. Results and discussion

The performance of SiO_2-supported nickel and iridium catalysts with different Ni/Ir molar ratios (Ni–Ir/SiO_2-X, X=Ni/Ir molar ratio) was investigated in hydrogenation of styrene as a model reaction. Ni-Ir/SiO_2 with Ni/Ir molar ratio of 1 (Ni-Ir/SiO_2-1) showed the highest conversion among the Ni-Ir/SiO_2-X catalysts, and the ethylbenzene was obtained in high selectivity (>99%). The reaction rate per total catalyst weight (160 mmol min^{-1} g^{-1}) is more than 7-fold higher than those of the monometallic counterpart catalysts (Figure 1). The reusability of the Ni-Ir/SiO_2-1 was confirmed by four-time reuse tests, and

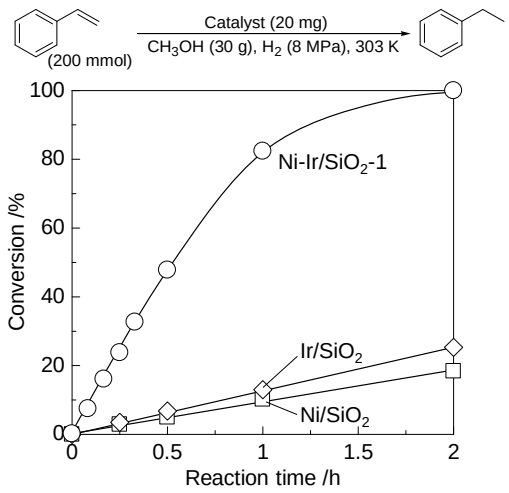

Figure 1 Time-courses of hydrogenation of styrene with Ni-Ir/SiO_2-1, Ir/SiO_2 (Ir: 4 wt%) and Ni/SiO_2 (Ni: 1.2 wt%) catalysts. Reaction conditions: catalyst 20 mg, styrene 200 mmol, CH_3OH 30 g, H_2 8 MPa, 303 K.

it was also confirmed that the catalyst structure was not changed during reaction by XRD and XAS analyses.

The characterization of Ni–Ir/SiO_2-1 by XRD, TPR, XAFS and TEM showed that the catalyst was composed of Ni–Ir alloys and Ni particles, and the average particle size of the Ni–Ir alloy was estimated to be ~3 nm (Figure 2). The alloy composition (Ni/(Ni+Ir)) of Ni-Ir alloy in Ni-Ir/SiO_2-1 catalyst was calculated based on Vegard's law to be 0.24 from the Ni-Ir alloy peak position of XRD patterns of Ni–Ir/SiO_2-1 catalyst, which was also supported by EDX line analysis of the TEM image (Figure 2).

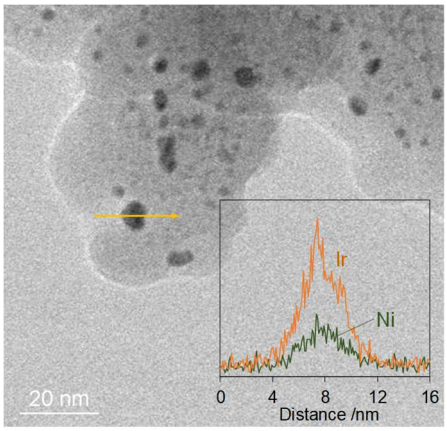

Figure 2 TEM image and EDX line analysis of Ni-Ir/SiO_2-1 catalyst after reduction.

The relationship between the turnover frequency based on the number of surface metal atoms (TOFs (min^{-1})) and alloy composition of Ni/(Ni+Ir) of Ni-Ir/SiO_2-X catalysts was investigated, and the result is shown in Figure 3. The TOFs increased with increasing the alloy composition up to 0.16, reaching a maximum TOFs of 4190 min^{-1}. However, the TOFs decreased at higher alloy compositions, suggesting that the high Ni content in the Ni-Ir alloys is not preferable for the reaction. The isolated Ni amount in Ni-Ir alloys with various Ni loading amount was estimated by the random model, which is called, ideal isolated Ni atom amount, and it is plotted as a function of the alloy composition of Ni/(Ni+Ir) (Figure 3). The change of the ideal isolated Ni amount is quite similar to that of the TOFs (Figure 3). These results strongly suggest that the isolated Ni atom in the Ni–Ir alloy can be the main active site for the reaction.

Finally, the applicability of the Ni-Ir alloy catalyst to hydrogenation of various unsaturated compounds was studied. Ni-Ir/SiO_2-1 showed higher activity to

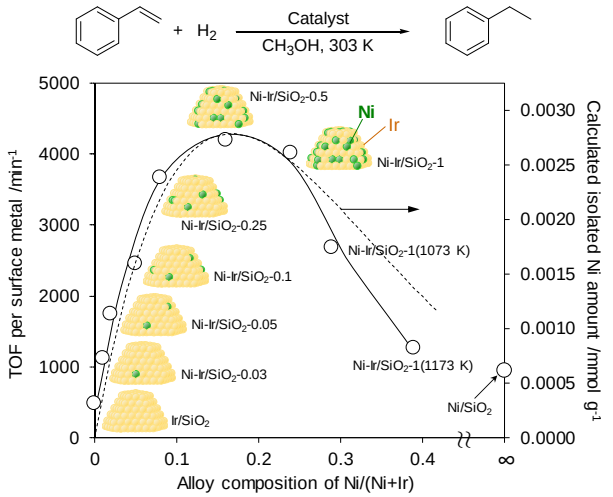

Figure 3 Relationship between alloy composition of Ni/(Ni+Ir) in Ni-Ir/SiO_2-X catalysts and TOF per surface metal (TOFs, solid line), ideal isolated Ni atom amount (dotted line) and images of alloys.

hydrogenation of various styrene derivatives with electron-donating and electron-withdrawing functional groups, 1-octene, a terminal olefin and 2-octene, an inner olefin, than the monometallic counterpart catalysts. On the other hand, the activity enhancement was not observed in hydrogenation of ethylbenezene, namely the catalyst is not suitable for hydrogenation of the aromatic ring. However, Ni-Ir/SiO_2-1 catalyst showed higher activity to hydrogenation of pyridine than the monometallic counterpart catalysts. The reaction mechanisms of hydrogenation of olefins, the benzene ring and pyridine ring over Ni-Ir/SiO_2 catalyst may be different. The details of the reaction mechanism will be discussed in the presentation.

We found that SiO_2-supported Ni-Ir alloy showed much higher activity for hydrogenation of olefins than the monometallic counterpart catalysts such as Ni/SiO_2 and Ir/SiO_2, and based on the catalyst characterization and kinetic studies, Ni single-atom in Ni-Ir alloy is responsible for the high activity.

This work was supported by Grand-in-Aid for Scientific Research on Innovative Area (18H04640) and Scientific Research (S) (18H05247) from JSPS.

1) P. Liu, Y. Zhao, R. Qin, S. Mo, G. Chen, L. Gu, D. M. Chevrier, P. Zhang, Q. Guo, D. Zang, B. Wu, G. Fu, N. Zheng, *Science*, 352 (2016) 797-801.

2) J. Bai, M. Tamura, Y. Nakagawa, K. Tomishige, *Chem. Commun.*, 55 (2019) 10519 - 10522.

Hydroxyapatite Supported Polyvinylpyrrolidone-Capped CuPd Bimetallic Catalysts for Highly Selective γ-Butyrolactone *via* Hydrogenation of Succinic Acid

(JAIST) ○LE, Dinh Son・NISHIMURA, Shun

1. Introduction

Succinic acid (SA) was identified as one of the most potential platform chemicals which can be converted to a number of value-added products.[1] The main types of SA conversions include hydrogenation, reductive amination, and esterification.[2] The catalytic hydrogenation toward γ-butyrolactone (GBL), 1,4-butanediol (BDO), and tetrahydrofuran (THF) is the most attractive conversion route; the manufacture of these expected to account for nearly one-third of the SA production in 2020.[3] In the present work, poly(*N*-vinylpyrrolidone) (PVP)-capped CuPd NPs stabilized on hydroxyapatite (HAP) is studied for the hydrogenation of SA to afford highly selective GBL.

2. Experimental

The Cu_xPd_y–PVP/HAP (x+y = 0.1 mmol) catalysts were prepared using polyol reduction method with 2-ethoxyethanol as a reducing agent. The catalysts were examined by extensive characterizations including X-ray diffraction (XRD), transmission electron microscopy (TEM), X-ray photoelectron spectra (XPS), and X-ray absorption fine structure (XAFS, Saga-LS, No. 1910092R).

Typically, a solution including 1,4-dioxane (10 mL), SA (0.1 g), and the catalyst (0.1 g) was loaded into an autoclave. The reactor was purged with pure H_2 before being pressurized to the target pressure at room temperature. Thereafter, the reactor was heated at 200 °C for 48 h under vigorous stirring. After reaction, the reaction media was centrifugated and analyzed by gas chromatography with a DB-FFAP column and a high-performance liquid chromatography using an Aminex HPX-87H column.

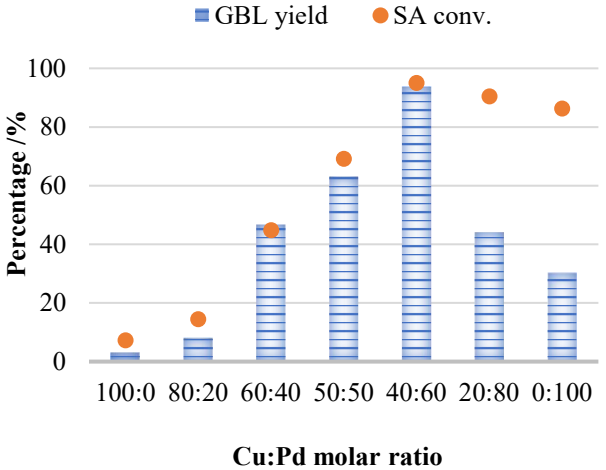

Figure 1. Effects of Cu:Pd ratio on the hydrogenation of SA over the Cu_xPd_y–PVP/HAP

3. Results and Discussions

Figure 1 shows the trend of hydrogenation of SA over the Cu_xPd_y-PVP/HAP with different Cu:Pd ratios. The monometallic Cu exhibited low activity, while the addition of Pd resulted in better catalytic performance; the SA conversion and GBL yield increased and reached its peak over the $Cu_{40}Pd_{60}$. Interestingly, further addition of Pd in this bimetallic system caused a significant drop in the GBL selectivity. The Pd monometallic catalyst exhibited lower activity and GBL selectivity. These results suggest that the close interaction between Cu and Pd, i.e., alloying, is responsible for the enhancement of catalytic activity and selectivity on the Cu_xPd_y–PVP/HAP catalyst.

The Pd-K edge XAFS results are shown in **Figure 2**. The monometallic Pd_{100} catalyst represents the Pd–Pd metallic peak of Pd foil at 2.74 Å. Upon addition of Cu, another peak was observed at lower position (2.54 Å), indicating the formation of Cu–Pd bonds of CuPd alloy.[4] Except for the Pd_{80} catalyst with low Cu concentration, the coordination numbers (CNs) of Pd–Cu increased with the increase of Cu concentration, indicating the increase in alloying degree. However, the Pd-Cu CNs did not explain the trend of catalytic performance for SA hydrogenation as shown in **Figure 1**. It is considered that the presence of isolated Pd in Pd rich CuPd alloy would account for the superior activity on the SA hydrogenation to highly selective GBL.

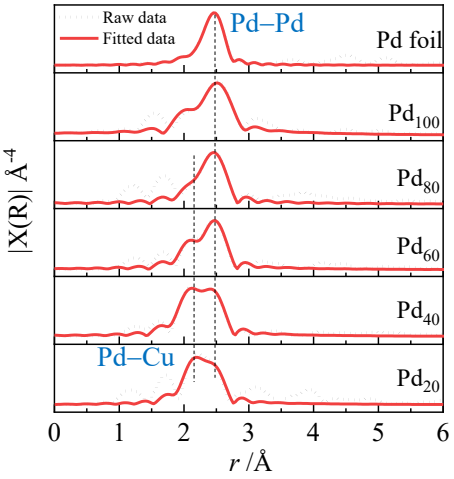

Figure 2. FT EXAFS fitting results at Pd K-edge.

1) A. Corma *et al.*, *Chem. Rev.*, **107**, 2411 (2007)
2) A. Mazière *et al.*, *Biofuels, Bioprod. Biorefining*, **11**, 908 (2017)
3) C. Delhomme *et al., Green Chem.*, **11**, 13 (2009)
4) F. Xing et al., *Chem. Sci.*, **10**, 8292 (2019)

Ultrastable and selective catalyst for propane dehydrogenation using Pb-modified PtGa alloy

(Hokkaido Univ.) Yuki Nakaya, Ken-ichi Shimizu, Shinya Furukawa

1. Introduction

Propylene is an important raw material for plastics, synthetic rubber, surfactants, dyes and pharmaceuticals. In recent years, there has been increased demand for propylene produced from cheaper, shale-originated propane. Reaction temperatures of more than 600°C are necessary to obtain sufficient propylene yields, but under these harsh conditions, severe catalyst deactivation is inevitable due to carbon deposition and/or sintering. Catalysts in practical use, therefore, must be regenerated continuously or in short cycles, making the process inefficient and costly.

In this study, we developed an ultrastable and selective catalyst for propane dehydrogenation using a Pb-modified PtGa alloy that worked for 96 h without deactivation even at 600°C.[1]

2. Experiment

Catalysts were prepared by co-impregnation method using silica (CARiACT G-6, Fuji Silysia) as a catalyst support (Pt loading: 3 wt%, Pt : Ga : Pb = 1 : 1 : 0.5). Propane dehydrogenation was carried out in a fix-bed continuous-flow reaction using quartz tube under atmospheric pressure at 600C (C_3H_8 : H_2 : He = 3.9 : 5 : 40 mL/min, catalyst: 15 mg, quartz sand 1.5 g).

3. Results and Discussion

Fig. 1 shows the catalytic performance of Pt-based catalysts. $PtGa/SiO_2$ and Pt_3Sn/SiO_2, which are known as selective catalysts for propane dehydrogenation, showed rapid deactivation within 10 h. In contrast, PtGa–Pb/SiO_2 retained the high propane conversion (30%) and propylene selectivity (99.6%) for 96 h (Fig. 2). The deactivation rate constant (kd) was 0.001 h^{-1}, which is the lowest value ever reported for propane dehydrogenation performed at >580°C. Thus, we successfully developed an ultrastable and selective catalyst for propane dehydrogenation.

FT-IR study with CO adsorption and DFT simulation for adsorbed CO revealed that (1)

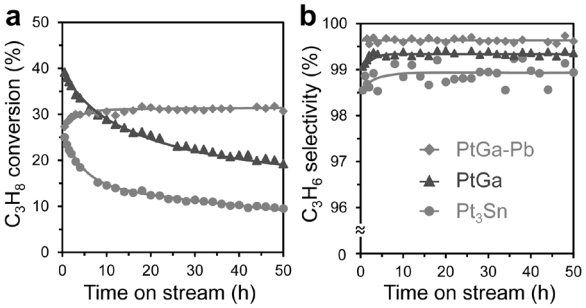

Fig. 1 Changes in propane conversion (**a**) and propylene selectivity (**b**) in propane dehydrogenation. Catalyst amount was adjusted so that the number of exposed Pt was identical (4.5 μmol): PtGa (9.0 mg), PtGa–Pb) (15 mg), Pt_3Sn (3.7 mg), and diluted with quartz sand (total 1.5 g). Gas feed: C_3H_8:H_2:He = 3.9:5.0:40 mL min^{-1}. Temperature: 600°C.

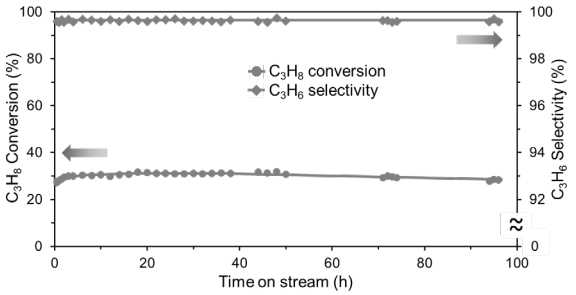

Fig. 2. Long-term stability test for PtGa–Pb/SiO_2.

PtGa alloys had single-atom-like isolated Pt_1 site surrounded by inert Ga and three-fold Pt_3 ensemble sites, and (2) the Pt_3 sites were selectively blocked by Pb deposition, while the Pt_1 sites remained intact. Comprehensive DFT calculation also indicated that the Pt_3 site was active not only for propane conversion to propylene but also for propylene decomposition, whereas Pt_1 site selectively catalyed propane conversion to propylene (propylene decomposition was effectively inhibited).

We also confirmed that the Pb-modified PtGa alloy nanoparticles were not sintered after the long-term use and the spent catalyst could be regenerated by O_2 treatment (calcination) and the subsequent H_2 reduction.

1. Y. Nakaya, J. Hirayama, S. Yamazoe, K. Shimizu, S. Furukawa, *Nat. Commun.*, **2020**, *11*, 2838.

インターナショナル sess.

[1E10-11] インターナショナル sess. 4

司会:西村 俊(北陸先端科学技術大学院大学)

2020年11月12日(木) 14:15 〜 15:00 E会場 (3F・中会議室E1-2)

[1E10] Synthesis of zeolitic Mo-doped vanadotungstate materials with tailorable oxidability and acidity

〇Tao Meilin[1]、Ishikawa Satoshi[1]、Ueda Wataru[1] （1. Faculty of engineering, department of material and life chemistry, Kanagawa University）

14:15 〜 14:30

[1E11] 酸化物ナノシートを用いたナノ構造触媒の開発

〇伊田 進太郎[1] （1. 熊本大学産業ナノマテリアル研究所）

14:30 〜 15:00

Synthesis of zeolitic Mo-doped vanadotungstate materials with tailorable oxidability and acidity

(Kanagawa Univ.) ○ TAO, Meilin・ ISHIKAWA, Satoshi・ UEDA, Wataru*

1. Introduction

Ordered porous transition metal oxides are more and more attractive because of their structure-based properties such as porosity and redox property. Previously, our group reported a kind of microporous zeolitic transition metal oxides ($W_{4.0}V_{3.0}O_{19}$; **VT-1**), which is composed of cubane clusters $[W_4O_{16}]^{8-}$ and VO^{2+} linkers (**Fig. 1**) [1]. Here we successfully prepared a series of transition metal substituted VT-1 materials, in which some of W in cubane unit was replaced by Mo, and V was substituted with Ti and Zr.

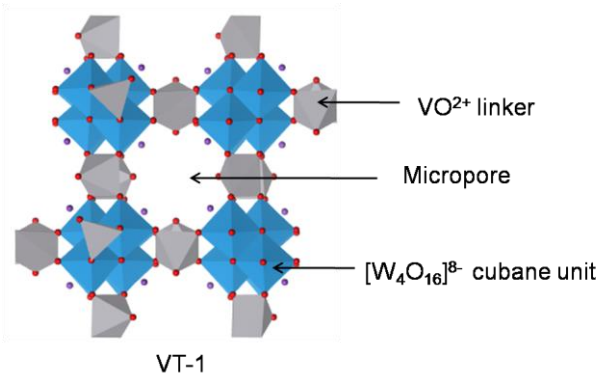

Fig. 1. Structural model of VT-1

2. Experimental

Mo_xW_{4-x} was obtained by hydrothermal synthesis (175 °C, 24 h) of the mixture of $(NH_4)_6H_2W_{12}O_{40}$, $(NH_4)_6Mo_7O_{24}$, and hydrated $VOSO_4$ under the pH of 4.0. $Mo_{0.7}W_{3.3}$(Ti or Zr)$_yV_{(3.0-y)}O_{19}$ were prepared by dispersing $Mo_{0.7}W_{3.3}$ in the aqueous solution of $Ti(SO_4)_2$ and $Zr(SO_4)_2$ with desired concentration.

3. Results and Discussion

From the ICP results, the addition of Mo caused the decrease of W in the unit cell, while the amount of V remained unchanged (**Fig. 2**). Based on DFT calculation, the stability of the Mo containing VT-1 materials decreased as the increase of Mo amount. The maximum doping amount of Mo was 1.0 ($W_{3.0}Mo_{1.0}V_{3.0}O_{19}$), and increasing Mo resulted in the formation of an unknown phase.

Then, we treated VT-1 and $Mo_{0.7}W_{3.3}$ with H_2SO_4 solution and the elemental compositions after the treatment were investigated by ICP (**Fig. 3a**). We found that the amount of V decreased with the decrease of pH

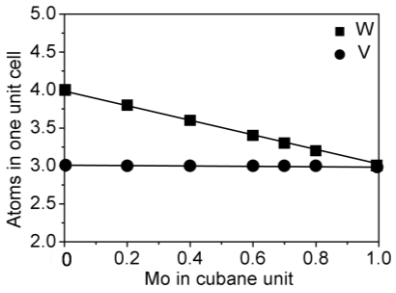

Fig. 2. The changes of W and V amount as a function of x in Mo_xW_{4-x} unit

in the solution and the rate of decrease of V was much faster in $Mo_{0.7}W_{3.3}$ than that of VT-1. We speculated that V in Mo_xW_{4-x} was leached out by hydration easier than that of VT-1 when decreasing the pH of the solution. The leaching of V from the structure caused the loss of the crystallinity as confirmed by XRD measurements. However, the crystallinity was remained unchanged when Ti or Zr source was added in the acid solution despite the leaching of V from the VT-1 structure. Interestingly, Ti or Zr was introduced into the VT-1 structure with the compensated amount of V leached out and the sum of V and Ti or Zr in the VT-1 structure was always 3.0, indicating that Ti or Zr is introduced into the V site leached out by the acid treatment (**Fig. 3b**). Maximum amount of Ti or Zr introducible into the structure was 1.0 in the VT-1 unit cell.

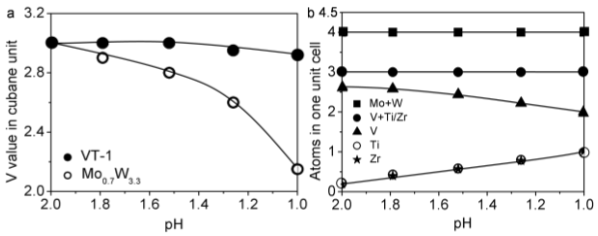

Fig. 3. Changes of the number of atoms in the VT-1 structure as a function of pH of the solution: a) in H_2SO_4 solution; b) in $Ti(SO_4)_2$ or $Zr(SO_4)_2$ solution.

FT-IR, Raman, and UV-Vis spectra further confirmed the successful introduction of Mo, Ti and Zr into the VT-1 structure. In the presentation, the physicochemical properties and catalytic activities over $Mo_xW_{(4-x)}$(Ti or Zr)$_yV_{(3.0-y)}O_{19}$ for NH_3-SCR will be discussed.

1) Z. Zhang, et al, *Nat. Commun*. **9**, 3789 (2018).

Development of nano-structured catalyst using oxide nanosheets

Kumamto Univerisity ○Shintaro Ida

Introduction

Some of layered compounds can be exfoliated into two-dimensional materials, so called nanosheets, with a thickness of around 1nm. Such nanosheets are used as building blocks to prepare well-ordered nano-structure such as super-lattice structure and pn-junction. In our study, we have been focusing on the activities of photocatalyst, and electrode catalyst of nano-structured catalysts prepared using nanosheets Hydrogen production from water using a photocatalyst and solar energy is the ultimate goal in renewable energy research [1]. Various oxides and oxynitrides have been reported as potential photocatalysts capable of decomposing water. However, there are several issues preventing their practical application, such as low quantum efficiency in the visible light region. One factor that causes a decrease in the photocatalytic activity is a recombination reaction between the electron and hole. When a photocatalyst is illuminated by light with an energy greater than the bandgap energy, a photo-excited electron and hole are generated within the powder. In order for these carriers generated within the powder to react with water, they must travel a long distance to the surface. During this trip, they may recombine or get trapped at defect sites. One ideal material that can suppress the recombination and provide a short travel distance is a semiconducting nanocrystal without inner and surface defects. However, in order to accomplish four-electron oxidation of water into oxygen on a 1 nm-diameter nanocrystal, one nanocrystal particle must absorb four photons with sufficient energy in a remarkably short time. Thus, it may be impossible to obtain sufficient photon flux density to meet requirements for solar energy.

A two-dimensional structure may satisfy the requirement described above. Specifically, a two-dimensional crystal (nanosheet) prepared by exfoliation of a layered compound is a single crystal with a homogeneous ultrathin thickness, and has a lateral dimension of several hundred nanometers to several micrometers. Therefore, the travel distance of the photo-excited carriers is short, and many photons can be absorbed by the nanosheet in a remarkably short time under low photon flux density due to its large section area. Recently, there have been many reports on p-type and n-type semiconducting nanosheets and nanosheet photocatalysts with visible light response, and studies on nanosheet photocatalysts have been becoming more frequent. The characteristic performance of nanosheet photocatalysts has been reported. For instance, it is well known that a photocatalyst without co-catalyst loading has poor photocatalytic activity for water splitting. However, a particular type of oxide nanosheet shows a high photocatalytic activity for hydrogen evolution from water without co-catalyst loading. A graphene-based photocatalyst is also a candidate photocatalyst, and new insights on photocatalytic reactions have been reported. Thus, the two-dimensional structure is expected to contribute to the development of photocatalysts for water splitting in the future. In this talk, e provides a short overview of recent research activities related to oxide nanosheets, nanosheet p-n junction photocatalysts [2], and attractive approaches for understanding the reaction mechanism [3], and electrode catalyst of nano-structured catalysts prepared using nanosheets.

Nanosheet p-n junction surface

The creation of a p-n junction is a strategy to improve photocatalytic activity, since the potential gradient generated by formation of a p-n junction can potentially act to suppress the recombination reaction. The potential gradient on the surface is generated by the diffusion of charge carriers between n-type and p-type semiconducting materials, which is expected to function as a driving force for the photo-excited holes and electrons to move to their respective reduction and oxidation sites. However, advancements in this field have been limited due to the difficulty in the preparation and evaluation of such junction structures. Nanosheets are a potential material to provide an answer to the issue mentioned above. A p-n junction structure without an amorphous layer between different p-type and n-type semiconducting materials with different crystal phases can be prepared by lamination of p-type and n-type semiconducting nanosheets. In the case of nanoparticles, the connection between them is point-to-point, whereas in a nanosheet, the connection is face-to-face. This is one of the advantages of nanosheets in the preparation of p-n junctions.

References:

[1] Takata, T., Jiang, J., Sakata, Y. *et al. Nature,* 581**,** 411–414 (2020).

[2] Awaya, K. Takashiba A., Taniguchi, T. *et al., Chem. Commun*., 55, 4586-4588 (2019,)

[3] Ida, S. Sato, K., Nagata, T., *et al., Angew. Chem. Int. Ed.,* 57, 9073-9077 (2018)

インターナショナル sess.

[2E01-03] インターナショナル sess. 5

司会:三浦 大樹(東京都立大学)

2020年11月13日(金) 09:00 〜 09:45 E会場 (3F・中会議室E1-2)

[2E01] ZSM-5担持 Rh二元機能触媒を用いた*n*-ヘキサン接触分解の低温化

○藤墳 大裕[1]、山地 真愛[1]、多湖 輝興[1] （1. 東京工業大学物質理工学院）

09:00 〜 09:15

[2E02] 高次な構造を有する Moおよび W酸化物触媒の合成と酸化触媒能

○下田 光祐[1]、宮沢 真維[1]、石川 理史[1]、上田 渉[1] （1. 神奈川大学工学部物質生命化学科）

09:15 〜 09:30

[2E03] フェノキシ配位ハーフチタノセン触媒によるエチレン共重合：活性への配位子効果

○Kitphaitun Suphitchaya[1]、野村 琴広[1] （1. 東京都立大学 理学研究科 化学専攻）

09:30 〜 09:45

Low temperature catalytic cracking of n-hexane over bifunctional catalyst containing Rh and ZSM-5

(Tokyo Inst. Tech.) ○Hiroyasu Fujitsuka, Mai Yamaji, Teruoki Tago

1. Introduction

Light olefins, such as propylene and butenes, are important chemical feedstock in petrochemical industry. They are generally produced from naphtha (C5~C8 paraffins and isoparaffins) by thermal cracking at around 800 °C or catalytic cracking over solid acid catalysts at around 650 °C[1]. These processes consume enormous energy due to high temperature operation and therefore the development of low temperature conversion process is required for energy saving. We have reported that bifunctional catalyst consisting of metal and solid acid could effectively convert naphtha at 400 °C because paraffins in naphtha were converted to C5~C8 olefins over metal catalyst which were easily converted to light olefins over solid acid catalyst[2]. In this study, the effect of distance between metal and solid acid in catalyst bed on the *n*-hexane cracking was investigated to optimize the catalyst bed structure for low temperature cracking of naphtha.

2. Experiment

Rh@ZSM-5 (bifunctional catalyst), Rh@Silicalite-1 (metal catalyst), and ZSM-5 (solid acid catalyst) were prepared in water-in-oil microemulsion solution as reported in the literature[3]. Three types of catalyst beds with different distance between metal and solid acid sites, defined as "intimacy criterion", were prepared (**Figure 1(a)**) and labeled as "layered", "granular-mixed", and "uniform" catalyst beds. In the layered catalyst bed, Rh@Silicalite-1 particle layer was placed onto ZSM-5 particle layer. The granular-mixed catalyst bed consisted of mixture particles of Rh@Silicalite-1 and ZSM-5. The uniform catalyst bed was prepared from Rh@ZSM-5. The amount of catalyst in bed was set at 0.2 g. Rh content and the Si/Al ratio in the catalyst bed were fixed at 0.3 wt% and 100, respectively.

The *n*-hexane conversion was performed at 400 °C using a fixed-bed flow reactor. The catalyst was pretreated in 10 % H_2/N_2 at 450 °C for 1 h. *n*-Hexane was supplied to the reactor accompanied by N_2 stream to adjust *W*/*F* value at 1.0 (kg-catalyst·h)/kg-*n*-hexane. The gas composition in the effluent of the reactor was analyzed by an on-line gas chromatograph.

3. Results and discussion

Figure 1(b) depicted the product yield of *n*-hexane cracking at 400 °C. All the catalyst beds showed larger conversion than that over ZSM 5 (less than 1 C-mol%), indicating that the combination of metal and solid acid promoted the *n*-hexane cracking at low temperature.

Among the catalyst beds tested, the uniform catalyst bed composed of Rh@ZSM-5 showed significantly higher conversion and olefin yield than the other catalyst beds tested. As shown in **Figure 1(a)**, metal and solid acid sites existed in the same zeolite particles for the uniform catalyst bed, and hence the intermediate olefins formed over metal was easily accessed the solid acid sites nearby. The synergetic effect of Rh metal and solid acid sites on *n*-hexane cracking was effectively obtained only when those sites were located close to each other (close intimacy).

Acknowledgement: This research is a part of technology development project conducted by JPEC commissioned by METI.

1) Sadrameli, S. M., *Fuel*, **173**, 285 (2016).
2) Yamaji, M. *et al*., 49th Petroleum-Petrochemicals Symposium of JPI, Yamagata, 2019, P18.
3) Fujitsuka, H. *et al*., *Catal. Today*, in press.

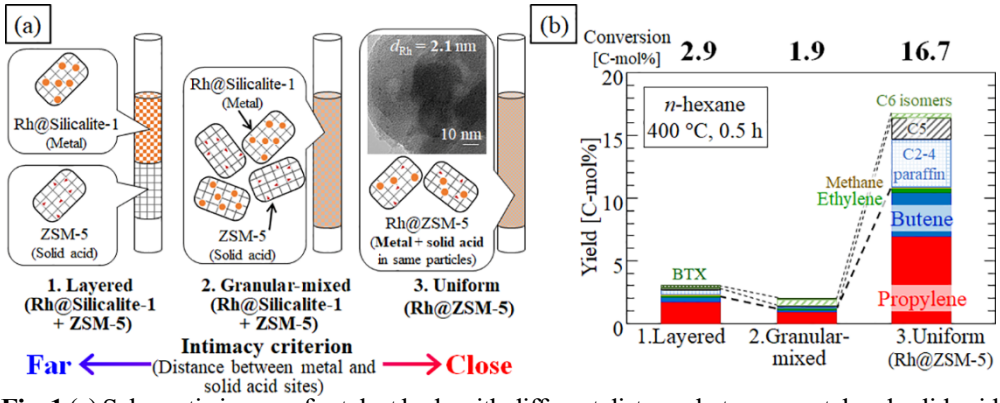

Fig. 1 (a) Schematic image of catalyst beds with different distance between metal and solid acid (b) *n*-hexane conversion over the catalyst bed at 400 °C for 0.5 h

Synthesis of High-Dimensionally structured Mo and W oxide and its oxidation properties

(Kanagawa University)○Kosuke Shimoda, Mai Miyasawa, Satoshi Ishikawa, Wataru Ueda.

1. Introduction

Crystalline Mo-V complex oxides (MoVO) are extremely active catalysts for selective oxidation of ethane and acrolein. MoVO is comprised of the structural arrangement based on pentagonal units $\{Mo_6O_{21}\}^{6-}$ and octahedral ($\{MO_6\}$, M=Mo, V), forming a basal which is stacked for each other to form rod-shaped crystals. The complex arrangement of the pentagonal units constructs micropore channels, such as hexagonal and heptagonal channels in the cross-section. Among these channels, the heptagonal channel is reported to work as catalysis field for selective oxidations. We recently obtained Mo and W oxides constituted by the structural arrangement of pentagonal units and octahedra, forming complex texture containing heptagonal channels in a similar manner to MoVO. In the presentation, we demonstrate details of the physicochemical and catalytic properties of the above Mo and W oxides.

2. Experimantal

High-dimensionally structured (HDS)-MoO_x was synthesized by hydrothermal synthesis using the precursor solution prepared by methyl ammonium heptamolybdate $(CH_3NH_3)_6Mo_7O_{24}$ (MAHM. Mo: 10 mmol) and molybdenum chloride $MoCl_5$ (Mo: 2.5 mmol). High-dimensionally structured (HDS)-WO_x was synthesized in a manner similar to HDS-MoO_x using the precursor solution prepared by ammonium metatungstate $(NH_4)_6[H_2W_{12}O_{40}]\cdot nH_2O$ (AMT. W : 10 mmol), tungsten chloride WCl_5 (W : 2.5 mmol) and trimethyl ammonium chloride (30 mmol). Hydrothermal synthesis was carried out at 175 °C for 20 h.

3. Results and Discussion

HDS-MoO_x and HDS-WO_x were obtained by hydrothermal synthesis of the precursor solution prepared by using the mixture of M^{6+} and M^{5+} sources (M = Mo, W) with appropriate alkylammonium cations as structure directing agents. These materials showed XRD peaks at 2θ = 22º and 46º attributable to the diffractions from (001) and (002) planes, indicating the periodic stacking of octahedral along the rod direction. We report that the materials showing the above two peaks belong to the family of HDS-oxides. Accordingly, we speculate that Mo and W oxides obtained here are the class of the HDS-materials. Figure 1 shows HAADF-STEM images of HDS-MoO_x and HDS-WO_x. These materials were rod-shaped crystals showing lattice fridge with the distance of ca. 0.40 nm, which is consistent with the *d* values measured by XRD. Due to the arrangement of the pentagonal units, hexagonal and heptagonal channels are formed in the cross-section. Heat treatment of these oxides resulted in the formation of oxygen vacancies as evidenced by O_2 pulse and TPO experiments. XPS and ORP experiments indicated that constituent elements were reduced with the formation of oxygen vacancies. If we assume that the elemental composition of HDS-(Mo or W)O_x is (Mo or W)O_3, these oxides retain the structure in the range of $MoO_{2.65\sim3}$ and $WO_{2.82\sim3}$. These feature might bring about attractive oxidation abilities derived from the oxygen vacancy and low-valence Mo and W species in the structure [1]. In order to investigate its oxidation ability, we carried out selective oxidation of isopropanol (C_3H_8O) (Table 1). Conventional Mo oxides such as α-MoO_3 and β-MoO_3 majorly afforded propylene (C_3H_6) in this reaction as a result of acid type reaction. On the other hand, HDS-MoO_x produced substantial amount of acetone (C_3H_6O) as a oxidation product than the conventional oxide catalysts.

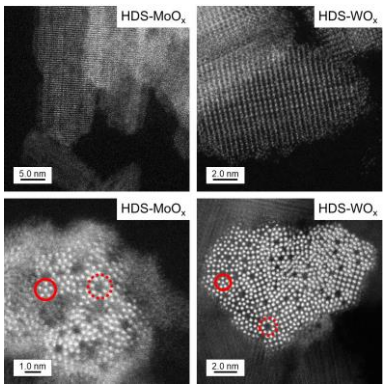

Figure 1. HAADF-STEM images of HDS-MoO_x and HDS-WO_x in side-section (upper) and cross-section (lower). Solid line, pentagonal unit; dotted line, heptagonal channel.

Table 1. Results of isopropanol oxidation

Sample	Conversion /%		Selectivity /%		
	C_3H_8O	O_2	C_3H_6O	C_3H_6	CO_x
HDS-MoO_x[a]	99.7	9.2	23.7	76.2	0.1
α-MoO_3[a]	99.4	4.4	1.0	98.9	0.1
β-MoO_3[b]	91.1	1.8	9.2	90.7	0.1

Reaction conditions. Catalyst amount(g). a; 0.05, b; 0.5, reaction gas; isopropanol/O_2/N_2 =1.5/3.0/20.0 mL/min, reaction temperature; 200 °C

1) E. W. McFarland, H. Metiu, *Chem. Rev. 113*, 4391 (2013)

Effect of *Para*-Substituent in Ethylene Copolymerizations Catalyzed by Phenoxy-Modified Half-Titanocene Catalysts

(都立大院理) ○Suphitchaya Kitphaitun, and Kotohiro Nomura*

1. Introduction

Introduction of polar functionality into polyolefin has been an attractive target due to promising properties expected with improvement in the surface nature and compatibility with other polymers. Half-titanocenes containing anionic donor ligands, Cp'TiX_2(Y), are known to be the efficient catalysts for synthesis of new polymers by ethylene copolymerization, and the ligand modification plays an important role.[1,2] We herein present our results for the synthesis of ethylene copolymers containing hydroxy group by incorporation of 9-decen-1-ol (DC-OH) in ethylene copolymerization with 1-decene (DC) using phenoxide-modified half-titanocenes Cp*$TiCl_2$(O-2,6-^{i}Pr_2-4-R-C_6H_2) [R = H (**1**), $SiMe_3$ (**2**), $SiEt_3$ (**3**)], in the presence of MAO (**Scheme 1**).[3]

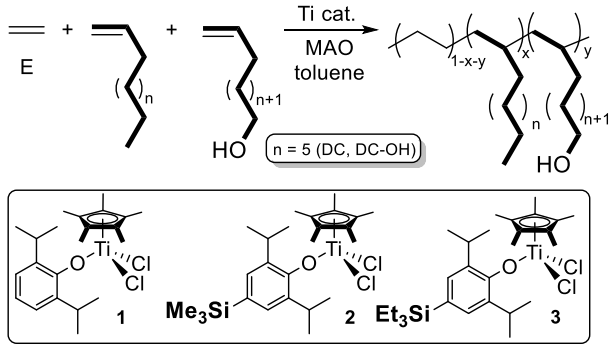

Scheme 1

2. Experimental

All experiments were carried out under a nitrogen atmosphere in a drybox or using standard Schlenk technique. Ethylene copolymerizations were conducted in toluene in the presence of MAO white solid (d-MAO), prepared by removing toluene and $AlMe_3$ in the commercially available sample [TMAO, 9.5 wt% (Al) toluene solution, Tosoh Finechem Co.]. Molecular weights and molecular weight distributions of the resultant polymers were analyzed by GPC and the microstructures were analyzed by NMR spectra.

3. Results and discussion

Selected results in ethylene/DC copolymerization in the presence of DC-OH by **1**-**3** (MAO cocatalyst) are summarized in **Table 1**. The results by linked half-titanocene, [$Me_2Si(C_5Me_4)(N^tBu)$]$TiCl_2$ (**4**) are also placed for comparison. It turned out that the $SiMe_3$ and the $SiEt_3$ analogues (**2**, **3**) exhibited higher catalytic activities than **1** and **4** (even in the absence of DC-OH or DC), notably at high temperature (50 and 80 °C). These catalysts afforded high molecular weight copolymers containing OH group with unimodal molecular weight distributions. Note that the activity by **3** increased upon increasing the DC-OH concentration whereas the activities by the others decreased under the same conditions. Noteworthy, the apparent decrease in the M_n value was not observed with increasing the DC-OH content (2.5 mol%). The hydroxy group in the resultant copolymer was treated with $AlEt_3$, and the subsequent ring-opening polymerization of ε-caprolactone afforded the grafting polymers with uniform molecular weight distributions. More details will be introduced in the symposium.

Table 1. Ethylene copolymerization with 1-decene (DC) and 9-decen-1-ol (DC-OH) by **1-4** – MAO catalysts.

cat. (μmol)	DC[c] / M	DC-OH[c] / M	activity[d]	M_n[e] ×10^{-4}	DC[f] / mol%	DC- OH[f] / mol%
1 (0.01)	0.79	0.093	31800	7.29	17.8	1.2
2 (0.01)	0.79	0.093	183000	7.58	15.0	1.5
3 (0.01)	0.79	0.093	47900	6.82	12.6	1.2
3 (0.01)	0.70	0.190	73200	6.70	14.1	2.5
3 (0.025)[b]	0.79	0.093	51800	2.65	14.1	0.8
4 (0.01)	0.79	0.093	6700	-	-	-
4 (0.01)	0.70	0.190	3100	-	-	-

[a]Conditions: total 30 mL, ethylene 6 atm, MAO 3.0 mmol, 50 °C, 10 min, Al^iBu_3 3.0 (DC 0.79 M) or 6.0 (DC 0.70 M). [b] At 80 °C, [c]Initial monomer concentration. [d]Activity in kg-polymer/mol-Ti·h. [e]GPC data in *o*-dichlorobenzene vs PS stds. [f]Comonomer content (mol%) estimated by ^{1}H NMR spectra.

References

(1) K. Nomura, *Dalton Trans*., 8811 (2009).
(2) K. Nomura, J. Liu, *Dalton Trans*., **40**, 7666 (2011).
(3) S. Kitphaitun, Q. Yan, K. Nomura, *Angew. Chem. Int. Ed.*, **59**, *ASAP* (2020).

